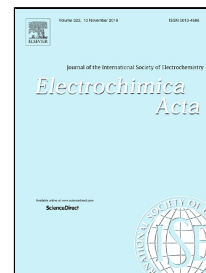# Journal Pre-proof

Electrochemical reduction of hematite-based ceramics in alkaline medium: challenges in electrode design

Daniela V. Lopes, Yu.A. Ivanova, Andrei V. Kovalevsky, Artur R. Sarabando, Jorge R. Frade, Margarida J. Quina

This is a PDF file of an article that has undergone enhancements after acceptance, such as the addition of a cover page and metadata, and formatting for readability, but it is not yet the definitive version of record. This version will undergo additional copyediting, typesetting and review before it is published in its final form, but we are providing this version to give early visibility of the article. Please note that, during the production process, errors may be discovered which could affect the content, and all legal disclaimers that apply to the journal pertain.

Electrochemical reduction of hematite-based ceramics in alkaline medium: challenges in electrode design

Daniela V. Lopes[1,2]*, Yu. A. Ivanova[1], Andrei V. Kovalevsky[1], Artur R. Sarabando[1], Jorge R. Frade[1], Margarida J. Quina[2]

[1]CICECO – Aveiro Institute of Materials, Department of Materials and Ceramic Engineering, University of Aveiro, 3810-193 Aveiro, Portugal

[2]CIEPQPF – Research Centre on Chemical Processes Engineering and Forest Products, Department of Chemical Engineering, University of Coimbra, Rua Sílvio Lima, 3030-790 Coimbra, Portugal

Abstract

Electrochemical reduction of low-conductive hematite-based ceramics represents a novel approach for iron recovery and waste valorisation. The process itself allows a flexible switching between hydrogen generation and iron reduction, important for the intermittent renewable-energy-powered electrolytic process. The present study focuses on the direct electrochemical reduction of aluminium-containing hematite in strong alkaline media. Within this scope, the reduction mechanisms of porous and dense cathodes, with 60%, 37% and 3% of open porosity, were investigated using different types of electrodes configuration: nickel-foil and Ag-modified nickel-foil supported configuration (cathodes facing or against the counter electrode), and nickel-mesh supported configuration. The efficiency of the iron reduction was compared for different electrode concepts. The results highlight the importance of electrolyte access to the interface between the metallic current collector and ceramic cathode for attaining reasonable electroreduction currents. Both excessively porous and dense ceramic cathodes are hardly suitable for such reduction process, showing a necessity to find a compromise between mechanical strength of the electrode and its open porosity, essential for the electrolyte access.

Keywords

Cellular ceramics; hematite; metallic iron; zero-valent iron; cathodic reduction

* Corresponding author
E-mail address: dvlopes@eq.uc.pt

1. Introduction

Iron oxides are available as natural raw materials and are also present in Fe-rich industrial wastes, such as red mud from the alumina refining industry. In the latter case, hematite is combined with other components, such as alumina, silica, calcium and magnesium oxides, requiring further separation from unwanted components and contaminants [1]. Metallurgical industry uses raw iron oxides for steel production and iron-based alloys by reduction in blast furnaces with carbothermal reducing agents resulting in massive CO_2 emissions. Thus, green alternatives to the traditional methods are gaining interest, such as electrochemical deposition of iron in acidic media [2,3], molten oxide electrolysis [4,5] and even iron pyroelectrolysis [6,7]. While some of these approaches require the use of high temperature, acidic conditions lead to looping between iron valences (Fe^{2+} and Fe^{3+}) and low process efficiencies [8,9].

Direct electrochemical reduction of iron oxides has been gaining attention [8–15] as a process allowing *in situ* reduction of the bulk ceramics at the cathode, under strong alkaline media. Despite 400 °C was used in the first attempts of hematite electroreduction to metallic iron [10], currently it is possible to apply lower temperatures (90 - 110 °C) using both bulk hematite or hematite particles in concentrated suspensions [14–17]. Such electrochemical reduction pathway also represents a new alternative for zero-valent iron (ZVI, Fe^0) production, which has been frequently used for environmental treatments based on the flexible interplay between the redox states [18]. However, existing challenges include insufficient current efficiency of this process at relatively low temperatures and inherent electrically insulating nature of iron oxides in these conditions, especially for hematite. Recent works focused on the studies of bulk electroreduction mechanisms of hematite to metallic iron and on general improvement of the relevant cathode electrochemical issues, in order to decrease hydrogen evolution and, consequently, increase current efficiencies. Conductive materials such as molybdenum [19], nickel [12,15] grids/wires/foils enfolded the cathode or were glued to it with conductive paste, to trigger the reduction of hematite. Porous structures of the bulk electrodes seem to enable the entrance of the electrolyte and, thus to facilitate the diffusion of electrochemically active

species. This fact was observed by Zou and his co-workers [15] when testing different sintering temperatures (700 - 1300 °C) for previously pressed Fe_2O_3 pellets. The higher residual porosity attained in the sample sintered at 1100 °C showed a pronounced impact on the reduction rate compared to the samples sintered at a higher temperature and possessing a lower residual porosity. However, lower sintering temperatures also lead to poor mechanical strength of the ceramics, showing the relevance of a balance between optimum sintering conditions for porosity, phase composition, and mechanical strength. Thus, an appropriate electrode design is especially important for facilitating the reduction of low-conductive ceramics, like hematite. A recent method for ceramics processing by the emulsification of ceramic powder suspensions [20–24] allows highly porous cellular microstructures, with interesting features for electrode applications. This approach was recently used for the first time for hematite [17] and hematite-based materials containing aluminium [25], and it was also used as precursors for cathodes in the present work. Ivanova et al. [17] obtained up to 64% of open porosity in hematite ceramics by applying various processing conditions. Three pellets with different open porosities levels (9%, 44%, and 64%) were tested as cathodes for electrochemical reduction at different experimental temperatures (25 °C and 90 °C) and different electrolyte concentrations (1 and 10 M of NaOH). The highest electrochemical activity towards iron reduction was observed for the ceramics possessing 64% of open porosity at 90 °C and in 10 M of NaOH proving that, besides the microstructural design of the electrode, the temperature and the basicity of the alkaline media have a significant impact on the efficiency of the process. However, a total conversion to metallic iron was not yet attained, and the faradaic efficiency was around 39%.

The possible presence of other components may impose even more limitations on the electrochemical bulk reduction of iron oxides. For example, aluminium may be present in noticeable amounts in both natural iron oxide ore and, especially, in industrial wastes like red mud. Straightforward studies of electrochemical reduction of the red mud are not expected to be conclusive enough regarding the relevant mechanisms of the process due to the inherent complex chemical and phase composition of the bauxite residue. In the present work, Al-substituted hematite ($Fe_{1.8}Al_{0.2}O_3$)

was tested as a model cathode material to assess the possible impacts provided by the aluminium presence. However, the particular novelty of this work is related to the assessment of different cathode concepts for the direct electrochemical iron reduction in alkaline medium, including various microstructural designs, supported configuration and preferred orientation towards counter electrode.

2. Experimental procedure

Hematite-based ceramics with designed porosity and containing a controlled addition of Al_2O_3, $Fe_{1.8}Al_{0.2}O_3$, were prepared by the emulsification of Fe_2O_3-Al_2O_3 powder mixture with liquid paraffin, using a procedure similar to that described in a previous work [25]. For the sake of comparison, dense pellets of the same composition were prepared by uniaxial pressing at 22 MPa. All samples were fired or sintered at 1100 °C and 1300 °C in air atmosphere (heating/cooling rates of 3 °C/min and 5 °C/min, dwell of 2 h). Open porosity of each sample was estimated by Archimedes method [21,25,26]. The fired ceramic samples retained a single phase solid solution, within the detection limits of XRD. Still, this is likely to be retained in a metastable condition, as found on extrapolating the boundaries of the single-phase region of the relevant phase diagram [27] to room temperatures.

Before electrochemical reduction tests, the samples were polished until a thickness between 1.5 – 3.0 mm and a geometrical area of around 0.7 cm^2, washed with distilled water and ethanol and dried in the oven. Silver paste (Agar Scientific) was used to glue Ni supports (foil and mesh, acting as a current collector) to the samples and provide reliable electrical contact. The area of Ni supports, which is not in the contact with the sample and exposed to the electrolyte was painted with lacquer (Lacomit Varnish, Agar Scientific) to avoid electrochemical contribution to the cathodic processes. After drying, the samples were soaked in the electrolyte (NaOH, 10 M) for 30 min to ensure a complete infiltration of the electrolyte inside of the porous cavities. Different electrode configurations with the prepared samples were tested. Table 1 presents those configurations and respective images of the electrodes. The $Fe_{1.8}Al_{0.2}O_3$ ceramics have a pellet form, with a lighter area corresponding to that covered with

4

silver. In "front" orientation the pellet was turned to the counter electrode by the open surface side, without Ag paste and/or lacquer; the "rear" orientation corresponds to 180° reversed configuration. It is important to note that Ag-modified designation is related to the pellet having one full face completely painted by Ag paste. In all cases, Ag paste is always locally glued to the Ni support to ensure electrical contact. NF (nickel foil) and NM (nickel mesh) configurations are shown in Table 1, with the cathode support covered with Teflon tape for isolation purposes. In the case of NMAg-R, the nickel mesh was used as a support and current collector, in order to ensure a better distribution of the current through the entire electrode surface as compared to NF configuration. The wires of the mesh without the contact with the ceramics were covered with lacquer. One face and the lateral sides of ceramics were also isolated with lacquer, and the only face of the ceramic electrode, covered with Ag paste, was exposed to the electrolyte.

[Here Table 1]

Electrochemical reduction studies were performed at 90 °C, with an Autolab potentiostat (PGSTAT 20) connected to the electrochemical cell in a Teflon reactor. A Pt wire was used as a counter electrode (CE) and Hg|HgO|NaOH (1 M) (+0.098 V versus saturated hydrogen electrode) as a reference electrode connected by a Luggin capillary to the electrolyte as previously described in [9,17]. Cyclic voltammetry (CV) was performed starting from the open circuit potential (E_{oc}) with a scanning rate of 10 mV/s. The current density values were calculated from the geometric area of each electrode. Amperometry curves were performed in potentiostatic mode at -1.075 V, unless indicated otherwise. Electrochemical impedance spectra (EIS) were registered in a frequency from 1 Hz to 1MHz, 50 mV of amplitude and 50 points per decade.

In order to perform a post-mortem analysis after electroreduction, the cathodes were washed with distilled water to remove the excess of NaOH and afterward preserved in ethanol. The morphology of the cathodes was studied by scanning electron microscopy (SEM) with a Hitachi S-4100 microscope, with chemical analysis by Energy-dispersive X-ray spectroscopy (EDS), model Bruker Quantax 400. The phase composition was assessed by X-ray diffraction with a PANalytical XPert PRO diffractometer
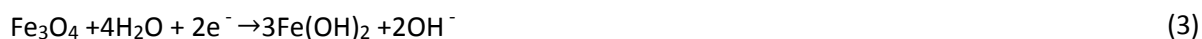
(CuKα radiation, 2θ = 10–80°) with a graphite monochromator. Phase content was calculated using Rietveld refinement procedure in Panalytical HighScore Plus 4.7 (PDF-4) software.

3. Results and discussion

3.1. Electrochemical behaviour of $Fe_{1.8}Al_{0.2}O_3$ electrode: general aspects

Cyclic voltammetry curves (CV) obtained for $Fe_{1.8}Al_{0.2}O_3$ cathodes with 60% of open porosity in NF-F configuration are shown in Fig. 1. This configuration is rather typical for the electroreduction studies in bulk ceramics [9,17], and gives some general guidelines regarding the electrochemical processes taking place at the cathode. Before electroreduction (Fig. 1A), a well-defined cathodic peak C_1 was detected at -0.97 V, while a poorly defined shoulder C_2 is superimposed on the hydrogen evolution region (E < -1.10 V). Higher cathodic polarizations than C_2 are associated with hydrogen evolution due to the water dissociation ($2H_2O + 2e^- \rightarrow H_2 + 2OH^-$). On the other hand, an anodic peak A_2 can be found at -0.65 V. A similar behaviour was observed in the voltammogram of Ivanova et al. [17], for Fe_2O_3 reduction with 64% of open porosity, in similar conditions (10 M of NaOH at 90 °C). One can assign the reduction of $Fe_{1.8}Al_{0.2}O_3$ (Fe_2O_3) to Fe_3O_4 and consequent reduction to Fe (II) to the peak C_1 ($C_1 \approx -1.00$ V in [17]) and reduction of Fe (II) to Fe^0 to C_2. Since there is no clear evidence from previous studies on the direct electroreduction of Fe_3O_4 to Fe^0 ($Fe_3O_4 + 8H^+ + 8e^- \rightarrow 3Fe^0 + 4H_2O$), as mentioned by Monteiro and co-workers [9], it seems plausible that a two-step reduction of $Fe_2O_3(Fe_{1.8}Al_{0.2}O_3) \rightarrow Fe_3O_4 \rightarrow Fe^{2+}$ takes place at potentials around C_1. One also assumes ready segregation of alumina from the metastable solid solution ($Fe_{1.8}Al_{0.2}O_3$) upon its partial reduction. Assuming this reduction mechanism, Fe_3O_4 dissolution in a strong alkaline medium (*e.g.* NaOH) can lead to the formation of iron hydroxides precursors (equations 1, 2, 3) [9]:

$$Fe_3O_4 + 4H_2O + OH^- + 2e^- \rightarrow 3Fe(OH)_3^- \tag{1}$$

$$Fe_3O_4 + H_2O + OH^- + 2e^- \rightarrow 3HFeO_2^- \tag{2}$$

6

$$Fe_3O_4 + 4H_2O + 2e^- \rightarrow 3Fe(OH)_2 + 2OH^- \tag{3}$$

It should be noticed that no C_2 shoulder was identified in the same CV spectrum in the work [17]. Since the CV scan from Fig.1A was obtained before the electroreduction of iron, the low definition of C_2 shoulder is related to the poor amount of Fe^0 reduced at that stage. At the reverse potential, the anodic peak A_1 is possibly related to the following oxidation of Fe (II) species (equations 4 and 5) [9,17,28]:

$$Fe(OH)_2 + OH^- \rightarrow FeOOH + H_2O + e^- \tag{4}$$

$$3Fe(OH)_2 + 2OH^- \rightarrow Fe_3O_4 + 4H_2O + 2e^- \tag{5}$$
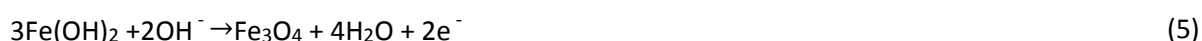
One can observe a significant increase in current density and only one cathodic peak at around -1.16 V (C_2), while also two anodic peaks at -0.82 V (A_2) and -0.56 V (A_1), when comparing the previous results with the voltammogram after reduction (Fig. 1B). An increase in the current density suggests a higher active surface area of the electrode [9], likely due to the presence of metallic Fe^0. After the electroreduction, C_1 peak disappears from the voltammogram, thus confirming the processes previously attributed to the peaks C_1 and C_2. The two anodic peaks are probably associated with the oxidation of Fe^0 to Fe (II) (A_2) and the oxidation of Fe (II) to FeOOH and/or Fe_3O_4 (A_1).

A cathodic and anodic peak can be found at potentials around 0.20 V (C') and 0.30 V (A'), respectively, in Fig. 1A. This behaviour can be associated with minor oxidation of the Ni foil used as cathode support in the electrochemical cell, to form $Ni(OH)_2$ and NiOOH, as observed at similar potentials by Skowroński and co-workers, in 6 M of KOH solution [29].

[Here Fig. 1]

The results of EIS studies performed for the same porous (60%) $Fe_{1.8}Al_{0.2}O_3$ electrode before electroreduction and after 2.5 h and 5 h of the reduction are shown in Fig. 2. The low-frequency semi-circle, corresponding to the mixed diffusion-controlled region, almost merges with high-frequency semi-circle, indicating the charge transfer processes, making difficult to extract the latter contribution. Therefore, the low-frequency part of the Nyquist plots was not considered for further analysis. The equivalent circuit used for EIS investigation is showed in the same figure, where the following

components are indicated: reference electrode (RE), resistance of solution/electrolyte (R_s), charge transfer resistance (R_1), double-layer capacitance (CPE_1) and working electrode (WE).

[Here Fig. 2]

Table 2 shows the corresponding fitting parameters, where true capacitance values, CPE_1 ($\alpha=1$), were calculated attending to equation (6):

$$C = ((R_1 x\ CPE_1)(R_1 x\ CPE_1)^{1/n})/R \qquad\qquad (6)$$

[Here Table 2]

Despite the low values of R_s, this parameter seems to decrease with time indicating some ohmic contribution between RE and WE before reduction. The charge transfer resistance R_1 dramatically decreases upon the reduction, likely due to the formation of a percolating network of the highly-conductive Fe^0 particles and, possibly Fe_3O_4. These results are in a good agreement with those obtained in [9]. CPE_1 ($\alpha=1$) values showed a significant increase from 0 to 5 h, which may indicate an expansion of the surface area of the WE due to the reduction to Fe^0, again in a good agreement with the same study.

3.2. Nickel-foil supported configuration

The CV curves shown in the Fig. 1A suggest that the iron reduction can be accomplished roughly in the cathodic potential range from -1.00 to -1.10 V, without risks of significant contribution from hydrogen evolution. Amperometry curves (currents vs. time) depicted in Fig. 3 were obtained for three different cathodic potentials (-1.00 V, -1.05 V and -1.10 V) during $Fe_{1.8}Al_{0.2}O_3$ reduction, in order to find a better estimation of another suitable potential for the cathodic reduction. Potential optimization also seems to be an important step to take into account when considering industrial needs, such as energy costs, suitable equipment for the range of potentials needed and time required for the electrochemical processes.

At lowest E = -1.00 V, the current density did not exceed the absolute value of -0.2 mA/cm² during 2.5 h, showing a weak tendency to increase. Thus, this cathodic potential was too low to promote

8

massive iron reduction and formation of more conductive phases than hematite [8,12,15,17]. By increasing the cathodic potential to E = -1.05 V, a slightly higher current density was observed ($\approx$ -1.0 mA/cm^2) at around 2.5 h of the reduction. At E = -1.10 V, a similar shape of the amperometry curve was observed. However, the current density increased considerably up to $\approx$ -24 mA/cm^2, which was the potential selected for the studies of iron oxide reduction in the Ni-foil supported configuration (NF).

[Here Fig. 3]

A comparative study of different NF configurations was thus undertaken at E_{cath} = -1.10 V (Fig. 4), corresponding denominations are described in Table 1. In general, the amperometry curves have a similar shape. A short-time decrease of the current density is observed during the initial stage of reduction, which can be attributed to the formation of an electric double layer at the cathode-electrolyte interface [30]. The decrease and increase of current densities around the same short period of time was observed in other studies [15,17], which may be associated with the entrance of the electrolyte inside of the electrode, where an interface between the current collector|solid insulator pellet|electrolyte (three phase interlines mechanism - 3PIs) starts to be formed [31,32]. Once the interface is formed near Ni current collector, the hematite-based $Fe_{1.8}Al_{0.2}O_3$ phase starts to be reduced forming more conductive phases, Fe_3O_4 and Fe^0, leading to an extension of the effective electrode area and increase of the cathodic current; this may explain the increase in nominal current density I/A_o, which is based on the initial electrode area A_o. In addition, volume changes on reducing hematite to metallic Fe^0 yield additional porosity, which also promotes further infiltration of the electrolyte inside the ceramic cathode. This minimizes ohmic losses by suppressing constrictions and also results in further increase of the current density (Fig. 4). In this case, the electrochemical reaction is self-sustained as long as the iron reduction takes place.

The NF-F configuration shows significant reproducibility, with current densities around -20 mA/cm^2 after 2.5 h of the reduction. On the contrary, NF-R configuration shows poor reproducibility: significant differences were found with the increase of the current density over time, where -13 mA/cm^2 (NF-R1)

9

and -37 mA/cm^2 (NF-R2) were obtained. However, the current densities in both NF-F tests are comparable with NF-R1. On the other hand, NF-R2 demonstrates a higher current density. Since the reduction starts at the interface between the current collector and $Fe_{1.8}Al_{0.2}O_3$ cathode, the configuration where the current collector is facing the counter electrode (NF-R) is expected to have a lower ohmic resistance and better current distribution after the initial reduction. The latter facilitates the electrochemical reduction, but can also result in losses of the mechanical integrity of the ceramic cathode. In particular, if few large pores with the access to the electrolyte are present at the interface between the current collector and $Fe_{1.8}Al_{0.2}O_3$ ceramics, this could result in very fast development of the reduction front, especially in the case of NF-R configuration. This might be responsible for high currents observed in the case of NF-R2 test.

[Here Fig. 4]

The above discussion of the cathodic processes during the electroreduction of $Fe_{2-x}Al_xO_3$ is further confirmed by the results of XRD and microstructural studies. Fig. 5 shows post-mortem studies of the NF-R electrode reduced at -1.10 V after 5 h. Ceramic cathodes can suffer significant physical stresses possibly due to pressure induced by hydrogen evolution, causing electrode delamination (Fig. 5), as the applied potential becomes cathodic relative to hydrogen evolution. In accordance with the XRD results (Fig. 5), Fe_3O_4 ($Fd\bar{3}m$) and Fe^0 ($Im\bar{3}m$) are found near the current collector (x). Indeed, SEM study reveals that large Fe^0 crystals (octahedron particles, d ≈ 3-12 μm) are present in the sample analysed near Ni foil and are incorporated in finer microstructures, probably, composed of Fe_3O_4. The initial cellular structure is not retained after reduction, suggesting that the reduction mechanism involves diffusion and re-deposition of the iron species from the electrolyte. Note also that the reduced regions only retain residual Al-rich spots. This confirms that electrolysis in alkaline conditions offers prospects for direct electrowinning of Fe^0 from $Fe_{2-x}Al_xO_3$ solid solution, without previous separation and with relatively low residual contamination with alumina.

When analysing a sample in the bulk away from the Ni current collector, Fig.5 (*), one can observe very few Fe^0 crystals and greater evidence of cellular cavities, resembling the initial microstructure. At

the same time, on the opposite side of the current collector (o), Fe^0 phase was not detected by XRD, and thus Fe_2O_3-type phase is likely the dominant compound, indicating the absence of reduction.

The results highlight not only the fact that the reduction starts at the interface between Ni and the ceramic electrode, but also that the combination of poor mechanical strength of the pellet and high cathodic potentials applied might be an issue for the electrode integrity. These guidelines are essential for cathode design and were taken into account in another configuration, namely, Ag-modified concept described in the next section, 3.3.

[Here Fig. 5]

3.3. Ag-modified nickel-foil supported configuration

This Ag-modified Ni-foil supported (NFAg) configuration is expected to be advantageous regarding the improvement of the contact area between the current collector and the electrode. Moreover, less porous, but mechanically stronger ceramic electrodes were used for testing this concept. Besides this, a lower cathodic potential was used in the reduction of the electrodes with Ag-modified configuration to further suppress the hydrogen evolution. The applied cathodic potential E_{cath} = -1.075 V was an intermediate value between conditions when current density was too low (at E = -1.05 V in Fig. 3) and conditions when hydrogen evolution may add difficulties (E = -1.10 V in Fig. 5). The present configuration was tested for $Fe_{1.8}Al_{0.2}O_3$ electrodes reduction, previously fired at 1300 °C, and retaining an intermediate value of porosity (37% of open porosity) in order to improve the mechanical strength. Amperometry curves are shown in Fig. 6, the cathodes were tested in NFAg-R (Fig. 6A) and NFAg-F (Fig. 6B) configurations. When using NFAg-R configuration, similar shape of the curves is observed when compared to the NF-R configuration. Since the face of the electrode with Ni-foil was completely painted with Ag paste and facing the counter electrode, more active surface for the electroreduction is available, leading to initial oscillations and higher currents over time. At 2.5 h, an increase of over 60% of the current density was observed for NFAg-R. One can distinguish three different periods on the current *vs* time dependencies during 5 h of the electroreduction. Namely, the

first period (until ≈ 2 h) dominated by electrolyte entrance in the electrode pores and the formation of 3PIs; in the second period ($\approx 2 - 4$ h), a maximum cathodic current is achieved (≈ -75 mA/cm^2 and -85 mA/cm^2), possibly due to almost complete reduction to Fe^0 in the locations with direct access to the electrolyte; and the third period (> 4 h), where a decrease of the current is noticeable and can be attributed to gradual exhaustion of precursor oxide in the ceramics bulk. Similar behaviour was observed in [15]. In fact, almost complete reduction of the NFAg-R electrodes was proved by XRD analysis (Fig. 6C), with a Faradaic efficiency close to 100%.

The front configuration NFAg-F is expected to provide better current distribution and more uniform reduction since the process starts at the interface between the current collector (Ni foil and Ag paste) and electrolyte. However, current oscillations occur on reaching nominal current densities of ≈ 80 mA/cm^2, (Fig. 6B), apparently as a result of less-homogeneous reduction, accumulation of stresses and partial disintegration of the electrode (Fig. 6C). Thus, Faradaic efficiency was not estimated for NFAg-F case due to the loss of a significant part of the ceramic electrode during the electrochemical tests.

[Here Fig. 6]

Fig. 7 shows the microstructural evolution of the $Fe_{1.8}Al_{0.2}O_3$ electrode in NFAg-R configuration. The electroreduction results in significant microstructural reorganization (Fig. 7B) as compared to freshly sintered ceramics (Fig. 7A). After 5h of electroreduction, one can observe only Fe^0 crystals (Fig. 7B), which is in agreement with the XRD studies (Fig. 6C). In fact, NFAg-R configuration allowed higher uniformity of electroreduction, as previously mentioned. Except for few bigger crystals (≈ 12 μm), the major part of Fe^0 is represented by smaller crystals (2 - 5 μm), also confirming a better homogeneity of the reduction in NFAg-R.

[Here Fig. 7]

Dense ceramic electrodes ($\approx 3\%$ of open porosity) of the same composition were also assessed in NFAg configuration to confirm the role of porosity on electrolyte access to the reaction sites. The results of amperometry studies are shown in Fig. 8. In general, significantly lower current densities are achieved when using dense $Fe_{1.8}Al_{0.2}O_3$ electrodes; this highlights the fact that, if using low-conductive

ceramics as a cathode, electrochemical reaction must occur at triple contacts, thus requiring access of the electrolyte to the interface between the ceramics and current collector; this determines the rate of the electrochemical reduction. Results in Fig. 8 also suggest that the NFAg-R configurations appear to outperform the NFAg-F configurations in terms of the current density. However, this is mainly found after major oscillations observed for NFAg-R2, likely originating from some pores and occasional defects, which may facilitate the electrolyte assess to the interface with the current collector. Once electroreduction is started in such discontinuities, this may add porosity in the reduced layer, activating new electrochemical sites and setting higher currents. Still, reproducibility of electroreduction of highly dense samples is poor in both "front" and "rear" configurations (Fig.8), possibly because faster electroreduction depends mainly on discontinuous residual porosity or other microstructural heterogeneities, as shown in Fig.9B, and also revealed by the diffused front between a fully reduced zone and a partially reduced front (Fig.9C).

[Here Fig. 8]

The XRD data and microstructural studies further confirm that the iron reduction takes place even in the case of the dense samples. Fig. 9 shows SEM micrographs of the initial $Fe_{1.8}Al_{0.2}O_3$ dense ceramics (Fig 9A), post-mortem analysis results (Fig. 9B,C) and corresponding XRD pattern (Fig. 9D). Microstructural changes after the reduction are clearly visible and, again, are localized at the interface between the current collector (Ag paste) and ceramics. In these places, the formation of Fe^0 crystals similar to those shown in Fig. 5 for NF-R configuration takes place (Fig. 9B). Better visualization of the reduction front is given on the cross-section SEM micrograph, showing a transition from rather porous reduced part to the dense non-reduced ceramics microstructure.

[Here Fig. 9]

3.4. Nickel-mesh supported configuration

Additional insight into the reduction mechanism in dense samples was obtained using a Ni-mesh supported electrode (NMAg-R), where the only surface of the ceramic electrode, exposed to the

electrolyte, was the one covered with Ag paste, in contact with Ni mesh. Within this concept, the electrolyte access was further minimized and restricted to the boundaries between Ni mesh wires, ceramics and Ag paste. The observed current densities are even lower than for NFAg configuration (Fig. 10A). As an example, around 3-times longer experiments were needed to achieve the currents comparable to those for NFAg (Fig. 8). Nevertheless, the amperometry curve shape suggests that the reduction still takes place in this configuration. When comparing the current density achieved in NFAg-F, one can suggest that the electrolyte diffusion through the lateral sides may significantly facilitate the process. This fact is highlighted by notably higher currents in the case of NFAg-R configuration. The microstructural results showed in Fig. 10B confirm the presence of reduction at the interface between the Ni-mesh current collector and the electrode (left part of Fig.10B), while the opposite side located 1.5 mm further apart from the Ni-mesh shows no sign of reduction (right side of Fig.10B). The reduction takes place at the whole surface, probably extending through a partially reduced layer with a typical thickness of about 20 μm, as revealed by differences in fracture cleavage at the surface layer marked by the yellow dash line in Fig.10B. On integrating the current density one would expect reduced layers with a typical thickness of about 50 μm, suggesting relatively low Faradaic efficiencies.

[Here Fig. 10]

4. Conclusions

Microstructural aspects of the ceramic electrodes and their configuration in the electrochemical cell were investigated and proved to play an important role for the electroreduction of the hematite-based $Fe_{1.8}Al_{0.2}O_3$ in strong alkaline media (10 M of NaOH, at 90 °C). Various ceramic electrode concepts were tested, including front and rear orientation towards counter electrode, deliberate exposing/blocking the access of the electrolyte and different ceramics porosity. The highlights of the present work consist of:

(1) the electrochemical tests of the dense and porous low-conductive electrodes, with 3%, 37% and 60% of open porosity, proved that the reduction is triggered at the interface between the current collector|$Fe_{1.8}Al_{0.2}O_3$ ceramics|electrolyte;

(2) the reduction of dense pellets was restricted to the area near Ni current collector, while the gradual self-propagation of the reduction front leads to nearly 100% Faradaic efficiency for the electrodes possessing 37% of open porosity;

(3) the parasitic contribution of the cathodic hydrogen evolution resulted in the collapse of ceramic electrodes with high open porosity (60%);

(4) electrowinning of dense samples was strongly affected by the electrolyte access through the lateral sides of the ceramic cathode or residual porosity at the propagation front.

Therefore, the novel methodology of direct electroreduction of Al-substituted hematite materials was proved to be successful for a complete reduction to Fe^0 or zero-valent iron with medium open porosities.

Acknowledgements

Declarations of interest: none

References
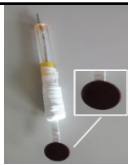
[1] M.A. Khairul, J. Zanganeh, B. Moghtaderi, The composition, recycling and utilisation of Bayer

red mud, Resour. Conserv. Recycl. 141 (2019) 483–498.

[2]   S.L. Díaz, J.A. Calderón, O.E. Barcia, O.R. Mattos, Electrodeposition of iron in sulphate solutions, Electrochim. Acta. 53 (2008) 7426–7435.

[3]   C. wei Su, F. jiao He, H. Ju, Y. bin Zhang, E. li Wang, Electrodeposition of Ni, Fe and Ni-Fe alloys on a 316 stainless steel surface in a fluorborate bath, Electrochim. Acta. 54 (2009) 6257–6263.

[4]   D.R. Sadoway, New opportunities for metals extraction and waste treatment by electrochemical processing in molten salts, J. Mater. Res. 10 (1995) 487–492.

[5]   H. Kim, J. Paramore, A. Allanore, D.R. Sadoway, Electrolysis of Molten Iron Oxide with an Iridium Anode: The Role of Electrolyte Basicity, J. Electrochem. Soc. 158 (2011) E101–E105.

[6]   N.M. Ferreira, A.V. Kovalevsky, S.M. Mikhalev, F.M. Costa, J.R. Frade, Prospects and challenges of iron pyroelectrolysis in magnesium aluminosilicate melts near minimum liquidus temperature, Phys. Chem. Chem. Phys. 17 (2015) 9313–9325.

[7]   N.M. Ferreira, A. V. Kovalevsky, M.C. Ferro, F.M. Costa, J.R. Frade, A new concept of ceramic consumable anode for iron pyroelectrolysis in magnesium aluminosilicate melts, Ceram. Int. 42 (2016) 11070–11076.

[8]   A. Allanore, H. Lavelaine, G. Valentin, J.P. Birat, F. Lapicque, Iron Metal Production by Bulk Electrolysis of Iron Ore Particles in Aqueous Media, J. Electrochem. Soc. 155 (2008) 125–129.

[9]   J.F. Monteiro, Y.A. Ivanova, A.V. Kovalevsky, D. Ivanou, J. Frade, Reduction of magnetite to metallic iron in strong alkaline medium, Electrochim. Acta. 193 (2016) 284–292.

[10]   K.H. Buob, A.F. Beck, M. Cohen, Study of the Cathodic Reduction of Oxide Films on Iron, J. Electrochem. Soc. 105 (1958) 74–78.

[11]   K.M. Gorbunova, L.I. Liamina, On the mechanism of iron reduction from alkaline solutions, Electrochim. Acta. 11 (1966) 457–467.

[12]   A. Allanore, H. Lavelaine, G. Valentin, J.P. Birat, P. Delcroix, F. Lapicque, Electrochimica Acta Observation and modeling of the reduction of hematite particles to metal in alkaline solution by electrolysis, Electrochim. Acta. 55 (2010) 4007–4013.

[13]   M. Tokushigea, O.E. Kongsteinb, G.M. Haarberg, Crystal Orientation of Iron Produced by Electrodeoxidation of Hematite Particles, ECS Trans. 50 (2013) 103–114.

[14]   Q. Wang, Y. Zhu, Q. Wu, E. Gratz, Y. Wang, Low temperature electrolysis for iron production via conductive colloidal electrode, RSC Adv. 5 (2015) 5501–5507.

[15]   X. Zou, S. Gu, X. Lu, X. Xie, C. Lu, Z. Zhou, W. Ding, Electroreduction of Iron (III) Oxide Pellets to Iron in Alkaline Media : A Typical Shrinking-Core Reaction Process, Metall. Mater. Trans. B. 46B (2015) 1262–1274.

[16]   Y.A. Ivanova, J.F. Monteiro, A.L. Horovistiz, D.K. Ivanou, D. Mata, R.F. Silva, J.R. Frade, Electrochemical deposition of Fe and Fe / CNTs composites from strongly alkaline hematite suspensions, J. Appl. Electrochem. 45 (2015) 515–522.

[17]   Y.A. Ivanova, J.F. Monteiro, L.B. Teixeira, N. Vitorino, A.V. Kovalevsky, J.R. Frade, Designed porous microstructures for electrochemical reduction of bulk hematite ceramics, Mater. Des. 122 (2017) 307–314.

[18]   F. Fu, D.D. Dionysiou, H. Liu, The use of zero-valent iron for groundwater remediation and wastewater treatment: A review, J. Hazard. Mater. 267 (2014) 194–205.

[19]   M. Gibilaro, J. Pivato, L. Cassayre, L. Massot, P. Chamelot, P. Taxil, Direct electroreduction of oxides in molten fluoride salts, Electrochim. Acta. 56 (2011) 5410–5415.

[20]   N. Vitorino, J.C.C. Abrantes, J.R. Frade, Cellular PCM / graphite composites with improved thermal and electrical response, Mater. Lett. 92 (2013) 100–103.

[21]   M.F. Sanches, N. Vitorino, J.C.C. Abrantes, J.R. Frade, J.B.R. Neto, D. Hotza, Effects of processing parameters on cellular ceramics obtained by paraffin emulsified suspensions, Ceram. Int. 40 (2014) 9045–9053.

[22]   N. Vitorino, C. Freitas, A.V. Kovalevsky, J.C.C. Abrantes, J.R. Frade, Cellular MgAl2O4 spinels prepared by reactive sintering of emulsified suspensions, Mater. Lett. 164 (2016) 190–193.

[23]   E. Lalli, N.M.D. Vitorino, J.G. Crespo, C. Boi, J.R. Frade, A.V. Kovalevsky, Flexible design of cellular Al2TiO5 and Al2TiO5-Al2O3 composite monoliths by reactive firing, Mater. Des. 131 (2017) 92–101.

[24]   N.M.D. Vitorino, A.V. Kovalevsky, M.C. Ferro, J.C.C. Abrantes, J.R. Frade, Design of NiAl2O4 cellular monoliths for catalytic applications, Mater. Des. 117 (2017) 332–337.

[25]   D.V. Lopes, A.V. Kovalevsky, M.J. Quina, J.R. Frade, Processing of highly-porous cellular iron oxide-based ceramics by emulsification of ceramic suspensions, Ceram. Int. 44 (2018) 20354–20360.

[26]   S.W. Hughes, Archimedes revisited: a faster, better, cheaper method of accurately measuring the volume of small objects, Phys. Educ. 40 (2005) 468–474.

[27]   M. Maruyama, T. Fukasawa, S. Suenaga, Y. Goto, Vapor-grown carbon nanofibers synthesized from a Fe2O3-Al2O3 composite catalyst, J. Eur. Ceram. Soc. 24 (2004) 463–468.

[28]   R.S. Schrebler Guzmán, J.R. Vilche, A.J. Arvía, The potentiodynamic behaviour of iron in alkaline solutions, Electrochim. Acta. (1979).

[29]   J.M. Skowroński, T. Rozmanowski, M. Osińska, Reuse of nickel recovered from spent Ni – Cd batteries for the preparation of C / Ni and C / Ni / Pd, Process Saf. Environ. Prot. 93 (2015) 139–146.

[30]   G. Wenjiao, C. Si, Y. Yanze, W. Hao, L. Jin, J. Yiming, Electrochemical impedance spectroscopy investigation on indium tin oxide films under cathodic polarization in NaOH solution, Thin Solid Films. 520 (2012) 6916–6921.

[31]   Y. Deng, D. Wang, W. Xiao, X. Jin, X. Hu, G.Z. Chen, Electrochemistry at conductor/insulator/electrolyte three-phase interlines: A thin layer model, J. Phys. Chem. B. 109 (2005) 14043–14051.

[32]   W. Xiao, X. Jin, Y. Deng, D. Wang, G.Z. Chen, Three-phase interlines electrochemically driven into insulator compounds: A penetration model and its verification by electroreduction of solid AgCl, Chem. - A Eur. J. 13 (2007) 604–612.

Figures and Tables

Table 1

Name	Configuration	Ag-modified	Sample orientation towards CE[1]	Sample type (porosity and processing conditions)	Scheme
NF-F	Ni-foil supported	No; Pellet borders and one face painted with lacquer	Front	Porous: 66%, T_{firing}[2] = 1100 °C 37%, T_{firing} = 1300 °C	
NF-R	Ni-foil supported	No; Pellet borders and one face painted with lacquer	Rear	Porous: 66%, T_{firing} = 1100 °C 37%, T_{firing} = 1300 °C	
NFAg-F	Ni-foil supported	Yes	Front	Porous: 37%, T_{firing} = 1300 °C Dense: 3%, T_{sint}[3] = 1300 °C	
NFAg-R	Ni-foil supported	Yes	Rear	Porous: 37%, T_{firing} = 1300 °C Dense: 3%, T_{sint} = 1300 °C	
NMAg-R	Ni-mesh supported	Yes	Rear	Dense: 3%, T_{sint} = 1300 °C	

CE[1] – counter electrode; T_{firing}[2] – firing temperature of the porous pellet; T_{sint}[3] – sintering temperature of the dense pellet.

Fig. 1.
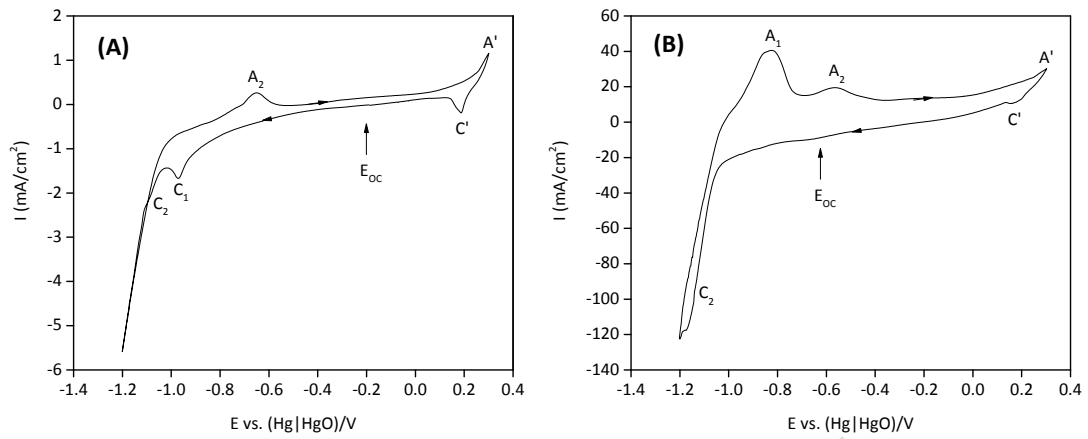
Fig. 2.
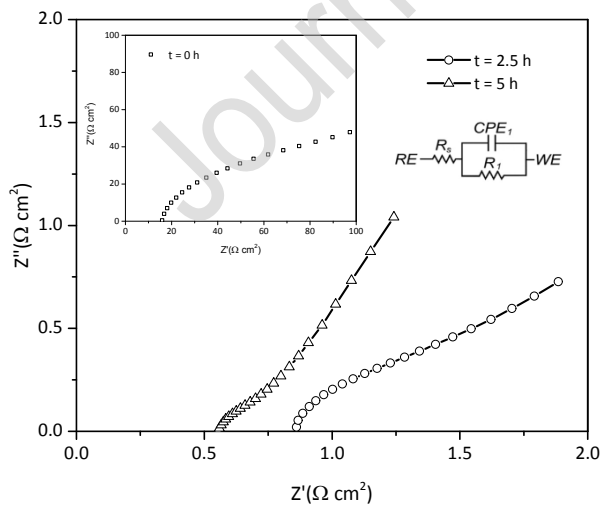
Table 2

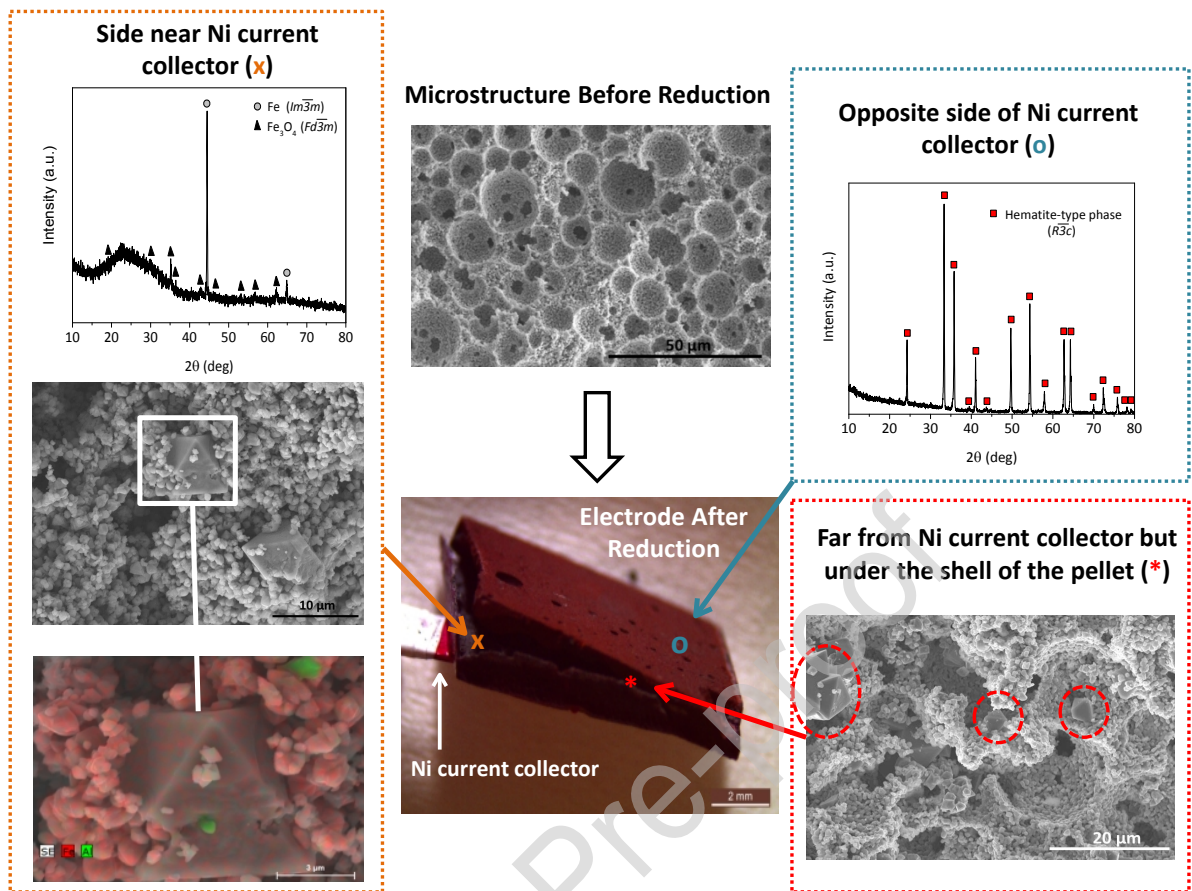| Time	R_s (Ω cm^2)	R_1 (Ω cm^2)	CPE$_1$ (α=1), μF/cm^2
t = 0 h	15.58	103.71	1.10×10^{-1}
t = 2.5 h	0.85	1.36	1.11×10^{3}
t = 5 h	0.55	0.69	5.60×10^{2}

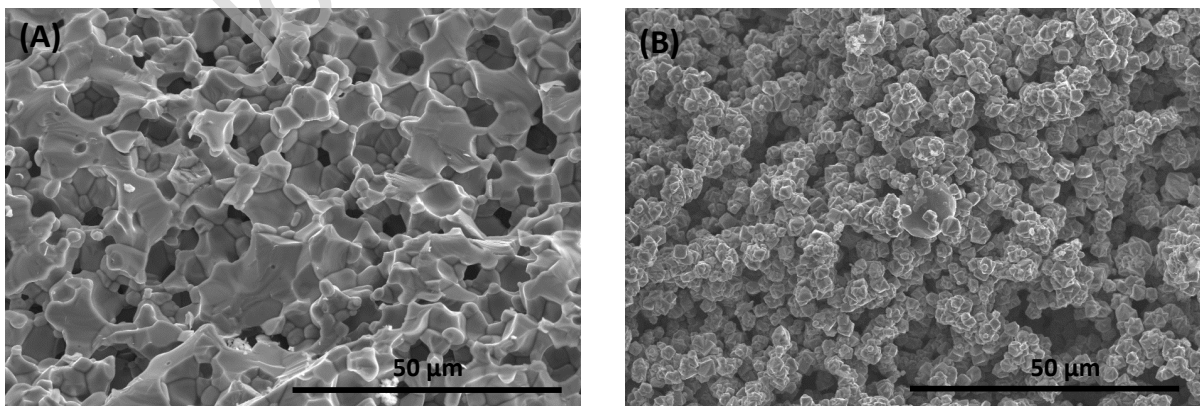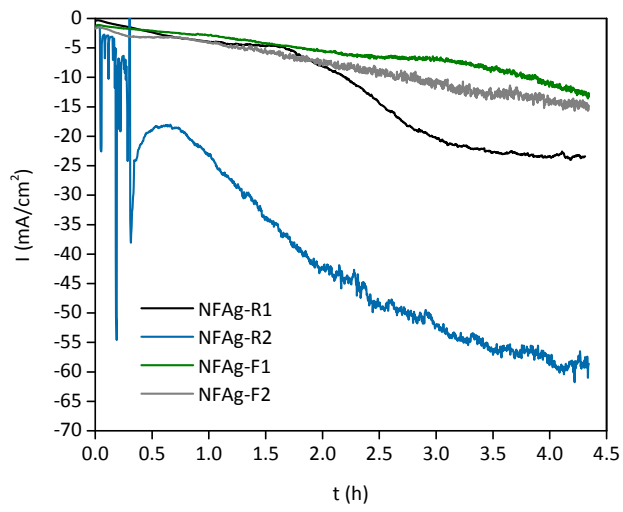Fig. 3.
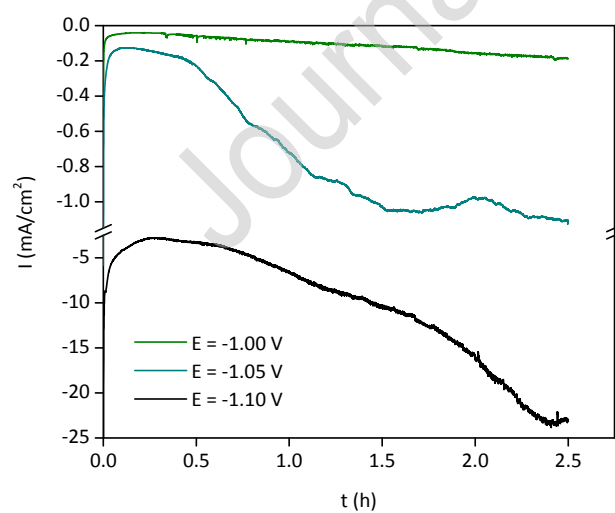
Fig. 4.
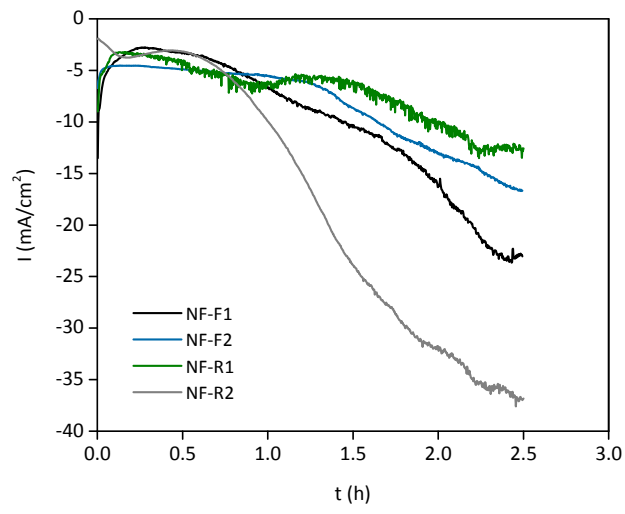
Fig.5.

Fig. 6.
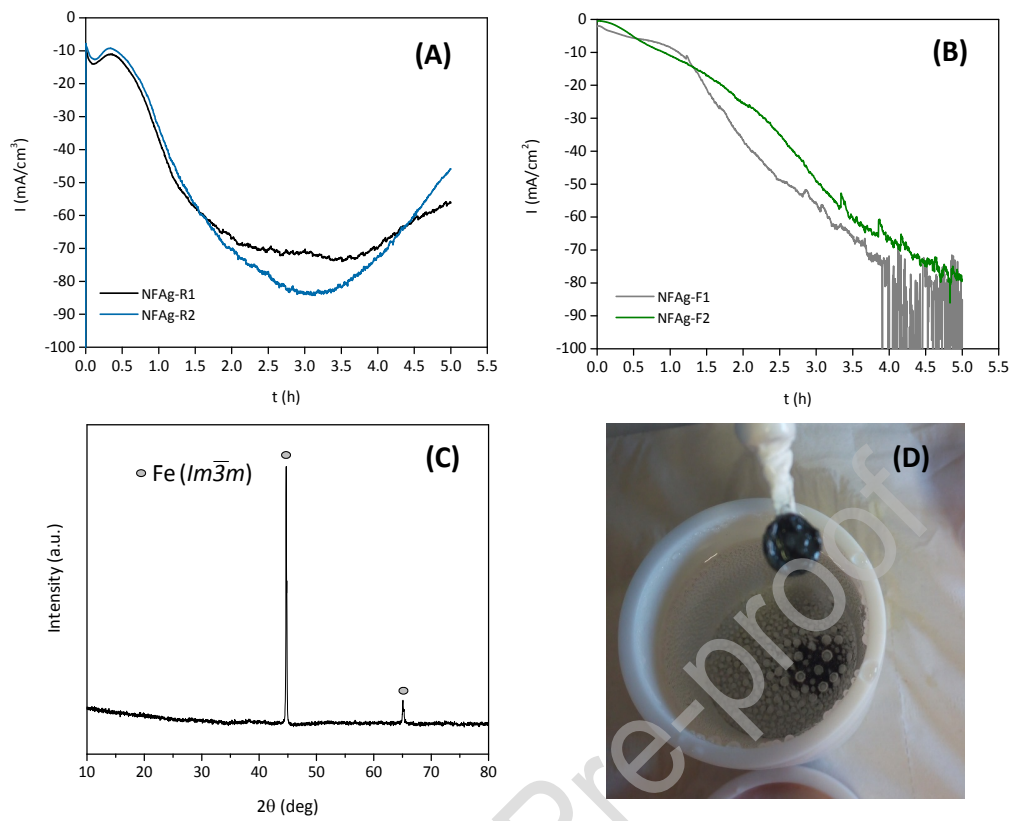
Fig. 7.
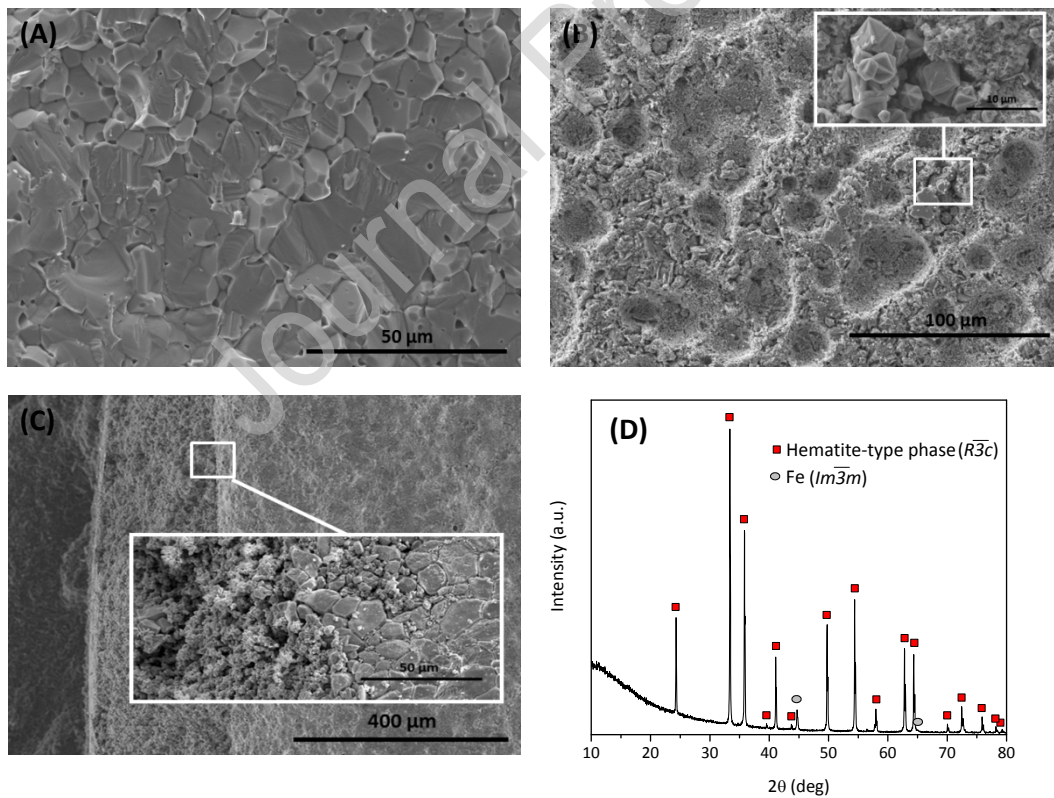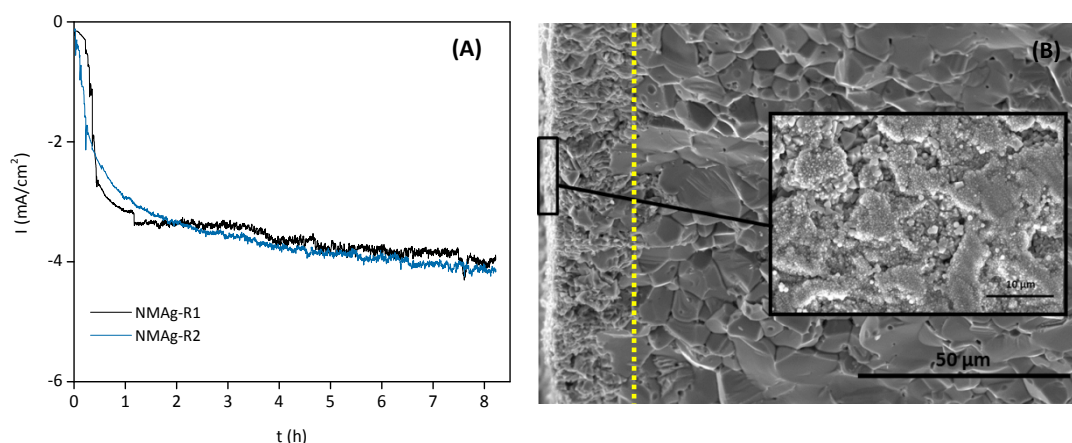
Fig. 8.

Fig. 9.

Fig. 10.

Captions of Tables and Figures

Table 1 – Electrode configurations studied.

Table 2 – Results of fitting of the EIS data: the parameters of the equivalent circuit.

Fig. 1. CV curves recorded with a scan rate of 10 mV/s for porous $Fe_{1.8}Al_{0.2}O_3$ (60% of open porosity) electrodes in 10 M NaOH at 90 °C in NF-F configuration before **(A)** and after **(B)** reduction at cathodic potential E_{cath} = -1.10 V.

Fig. 2. Nyquist plots for non-reduced 60%-porous $Fe_{1.8}Al_{0.2}O_3$ sample (t = 0 h) and the same sample reduced during t = 2.5 h and t = 5 h at E_{cath} = -1.10 V (NF-F electrode configuration) at 90 °C in 10 M NaOH.

Fig. 3. Current vs. time curves at various cathodic potentials (-1.00 V, -1.05 V and -1.10 V) for 2.5 h (60% of open porosity).

Fig. 4. Current-time transients recorded for NF-F and NF-R configurations at E_{cath} = -1.10 V for 2.5 h (60% of open porosity).

Fig. 5. Post-mortem studies of the NF-R electrode (60% of open porosity, E_{cath} = -1.10 V, 5 h of reduction).

Fig. 6. Reduction of $Fe_{1.8}Al_{0.2}O_3$ electrode (37% of open porosity, 5 h), previously fired at 1300 °C, with E_{cath} = -1.075 V in different orientations towards CE: (A) NFAg-R and (B) NFAg-F; (C) XRD analysis of NFAg-R test; (D) pellet collapse during NFAg-F test.

Fig. 7. Microstructural evolution after electroreduction of the electrode in NFAg-R configuration: (A) before reduction (37% of open porosity); (B) after 5 h of reduction (bulk of the electrode).

Fig. 8. Current-time transients obtained for dense $Fe_{1.8}Al_{0.2}O_3$ samples (3% of open porosity), E_{cath} = -1.075 V, in NFAg-R and NFAg-F electrode configuration.

Fig. 9. SEM microstructures of dense $Fe_{1.8}Al_{0.2}O_3$ electrode in NFAg-R configuration (A) before reduction (3% of open porosity); and after reduction (E_{cath} = -1.075 V): (B) under the Ag layer near the Ni current collector; (C) cross-section starting from the current collector left to the ceramics bulk (right) (D) XRD pattern obtained for the whole ceramic electrode converted to powder.

Fig. 10. (A) Current *vs.* time curves obtained for NMAg-R configuration at E = -1.075 V, using a dense electrode (3% of open porosity); (B) SEM images of the microstructural alteration in the cross-section of the electrode: at the surface beneath the Ag paste in the contact with Ni-mesh and electrolyte (left part) and structure without reduction (right part).